

Prediction of the Weyl semimetal in the orthorhombic MoTe₂

Yan Sun¹, Shu-Chun Wu¹, Mazhar N. Ali², Claudia Felser¹, and Binghai Yan^{1,3,4,5*}

¹Max Planck Institute for Chemical Physics of Solids, 01187 Dresden, Germany

²IBM Almaden Research Center, San Jose, California 95120, USA

³Max Planck Institute for the Physics of Complex Systems, 01187 Dresden, Germany

⁴School of Physical Science and Technology, ShanghaiTech University, Shanghai 200031, China and

⁵CAS-Shanghai Science Research Center, Shanghai 201203, China

(Dated: September 30, 2015)

We investigate the orthorhombic phase (Td) of layered transition-metal-dichalcogenide MoTe₂ as the Weyl semimetal candidate. MoTe₂ exhibits four pairs of Weyl points lying slightly above (~ 6 meV) the Fermi energy in the bulk band structure. Different from its cousin WTe₂ that was predicted to be a type-II Weyl semimetal recently, the spacing between each pair of Weyl points is found to be as large as 4 percent of the reciprocal lattice in MoTe₂ (six times larger than that of WTe₂). When projected to the surface, Weyl points are connected by Fermi arcs, which can be easily accessed by ARPES due to the large Weyl point separation. In addition, we show that the correlation effect or strain can drive MoTe₂ from type-II to type-I Weyl semimetal.

I. INTRODUCTION

The Weyl semimetal (WSM) is a topological semimetal¹⁻³, in which bands disperse linearly in three-dimensional (3D) momentum space through a node, called Weyl point (WP). The WP acts as a monopole with fixed chirality⁴, a source or a sink of the Berry curvature. Similar to those of a topological insulator (TI), topologically protected surface states exist on the surface of a WSM. Topologically different from ordinary Fermi surfaces (FSs), these surface states present unclosed FSs, called Fermi arcs, which connect the surface projections of WPs with the opposite chirality². WSMs also exhibit exotic quantum transport phenomena, such as the chiral anomaly⁵⁻⁷ characterized by the negative longitudinal magnetoresistance (MR)⁸, anomalous Hall effect^{3,9-11} and nonlocal transport properties^{12,13}.

Recently the first WSM materials (Ta,Nb)(As,P) have been discovered by addressing the Fermi arcs in angle-resolved photoemission spectra (ARPES)¹⁴⁻²⁰, which was originally predicted by band structure calculations^{21,22}. Meanwhile a great amount of efforts have also been devoted to their magneto-transport properties²³⁻²⁹, such as extremely large, positive transverse MR²³ and large, negative longitudinal MR^{24,29}. These family of WSMs exhibit ideal Weyl cones in the bulk band structure, i.e. the FS shrinks into a point at the WP. Very recently, Soluyanov *et al.* proposed a new type of WSM in the compound WTe₂³⁰, referred as type-II WSM³¹. Herein, the Weyl cone is strongly tilted so that WP exists at the touching point of the electron and hole pockets in the FS, which may indicate salient response to the magnetic field. Topological Fermi arcs were demonstrated between a pair of WPs that are separated by $\sim 0.7\%$ of the reciprocal lattice vector length and lie about 50 meV above the Fermi energy (E_F).

Provoked by WTe₂³¹, we predict that the orthorhombic phase of MoTe₂, which was synthesized very recently³², is a new type-II WSM candidate. The layered transition metal dichalcogenide MoTe₂ can crystallize into

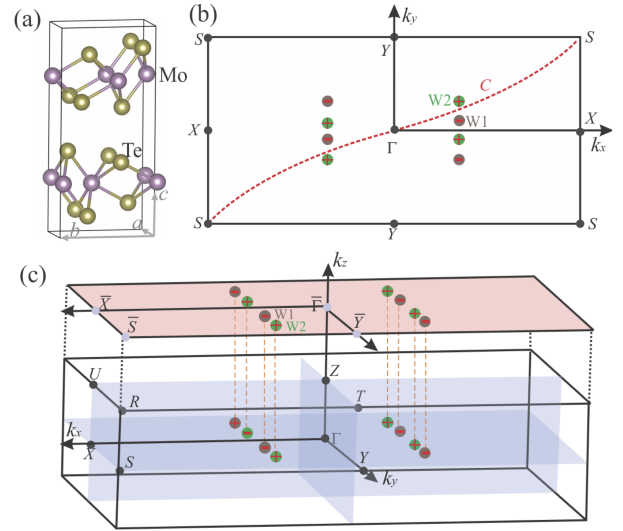


FIG. 1. (color online) (a) Orthorhombic crystal lattice structure of Td-MoTe₂ in the space group of Pnm2₁. (b) Brillouin zone (BZ) in the $k_z = 0$ plane. WPs with positive and negative chiralities are marked as green and gray dots. The evolution of Wannier charge centers between Γ to S point is calculated along the red curve C . (c) 3D bulk BZ and the projected surface BZ to (001) plane.

three phases in different experimental conditions: the 2H, 1T' and Td phases. The 2H phase is semiconducting, in which the Mo atom has trigonal prismatic coordination with the Te atoms. The 1T' (also called β -phase)³³ and Td phases are semimetallic and exhibit pseudo-hexagonal layers with zig-zag metal chains. The 1T' phase is a monoclinic lattice that is stable at room temperature, arising from the slight sliding of layer-stacking of the orthorhombic lattice of the Td phase (see Fig. 1a). The Td compound can be obtained by cooling the 1T' phase down to 240 K^{32,34,35}. We note that the 1T' structure exhibits inversion symmetry (space group $P12_1/m1$, No. 11) while

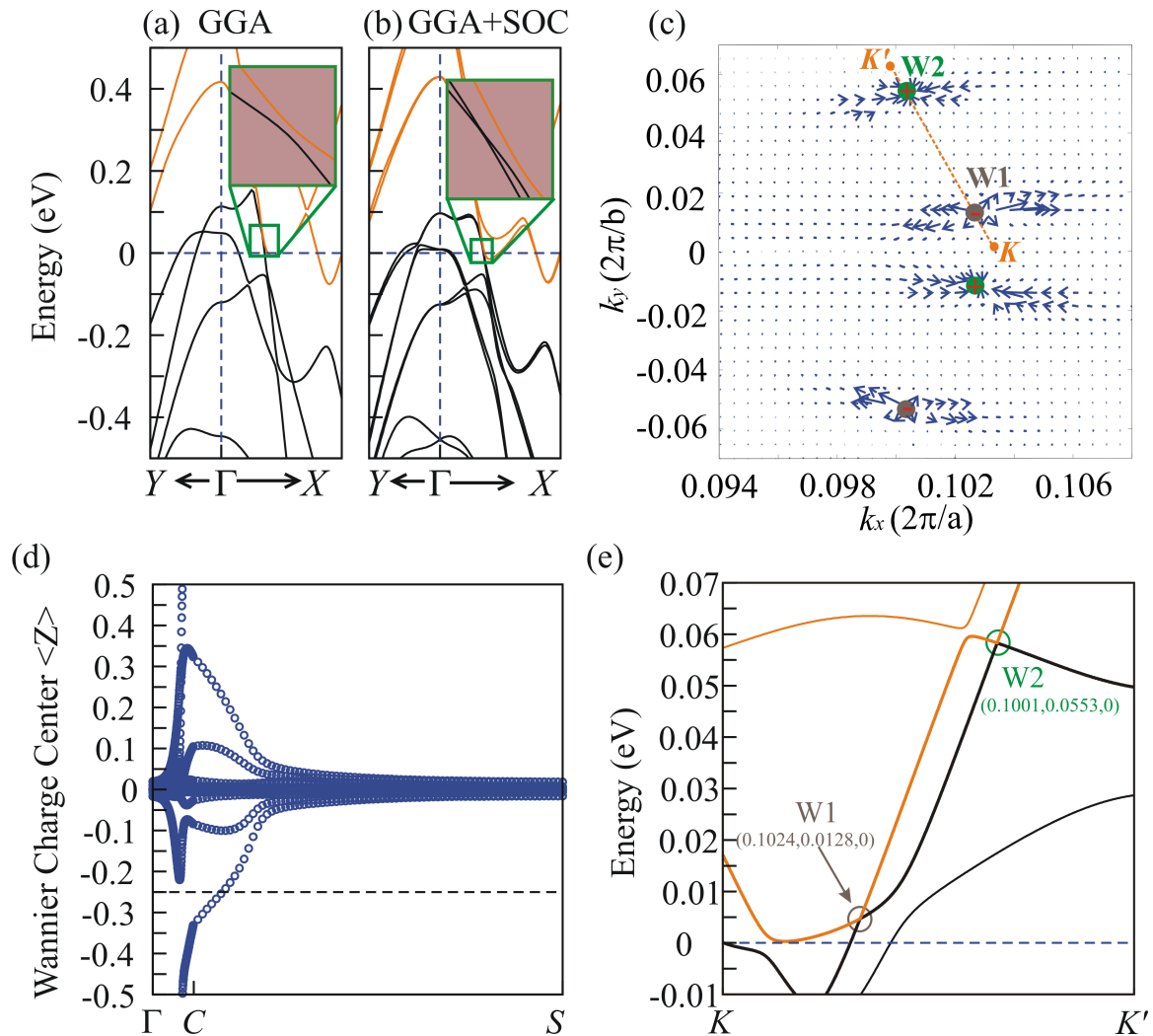


FIG. 2. Bulk band structure around Γ point in the direction of $Y - \Gamma - X$ direction (a) without and (b) with the inclusion of SOC. (c) Berry curvature in the $k_z = 0$ plane around two types of WPs. The size and directions of arrows represent the magnitude and orientations of the Berry curvature, respectively. WPs with positive and negative chirality are denoted by the green and gray points. (d) The evolution of Wannier charge centers between two time-reversal-invariant points of Γ and S along the C curve (see Fig. 1b). The Wannier charge centers cross the reference horizontal line once, indicating the nontrivial Z_2 invariant in the C - k_z plane. (e) Band structure crossing two types of WPs. The two points of K and K' is shown in (c). Black and orange bands in (a), (b) and (e) are the lowest N -th bands and other higher bands, respectively.

the Td one does not (space group $Pmn2_1$, No. 31). The $1T'$ phase of MoTe_2 was speculated to be a WSM candidate as a pressurized WTe_2 in Ref. 31. We note that, however, the $1T'$ phase cannot be a WSM simply because of the co-existence of time-reversal symmetry (TRS) and the inversion symmetry, because the WSM requires the breaking of at least one of the TRS and inversion symmetry. Therefore, only the Td phase, which is isostructural to WTe_2 , can be a possible WSM.

In this work, we have investigated the Td- MoTe_2 as a WSM candidate by *ab initio* density-functional theory (DFT) calculations. We indeed find four pairs of WPs in the band structure (see Fig. 1c), similar to WTe_2 . Each pair of WPs exhibit considerable spacing in the

Brillouin zone, $\sim 4.2\%$ of the reciprocal lattice vector, in which one WP exists merely 6 meV above E_F and the other WP lies 59 meV above E_F . We observe clear Fermi arcs in the surface state calculations. Due to the large momentum spacing and the close vicinity to E_F of WPs, we expect that the Fermi arcs and other interesting quantum phenomena of MoTe_2 will be easily accessed by future ARPES and transport experiments.

II. METHODS AND CRYSTAL STRUCTURE

DFT calculations were performed with the Vienna *Ab initio* Simulation Package (VASP)³⁶ with projected

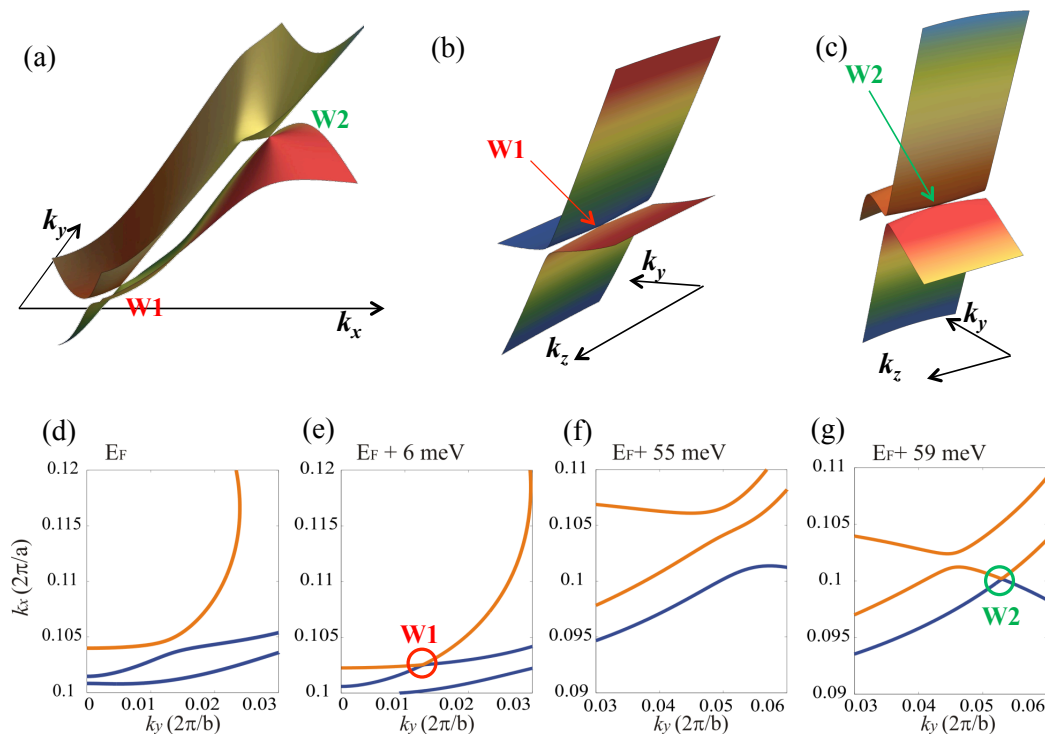


FIG. 3. 3D plot of WPs in (a) $k_z = 0$, (b) $k_x = 0.1024 \frac{2\pi}{a}$ and (c) $k_x = 0.1001 \frac{2\pi}{a}$ planes. (d-g) The evolution of FS around two WPs in $k_z = 0$ plane. WPs related Fermi surface linear crossing can be at $E_F + 6$ meV and $E_F + 59$ meV, respectively. The orange and blue FSs come from the electron and hole pockets.

augmented wave (PAW) potential. The exchange and correlation energy was considered in both generalized gradient approximation (GGA)³⁷ level with Perdew-Burke-Ernzerhof (PBE) functional and hybrid functional (HSE06)³⁸. The energy cutoff was set to 300 eV for a plane wave basis. The tight-binding matrix was constructed by projecting the Bloch states into maximally localized Wannier functions (MLWFs)³⁹. We employed the experimental lattice parameters and atomic positions measured by our recent experiment³². For completeness, the lattice constants are $a = 3.477\text{\AA}$, $b = 6.335\text{\AA}$, and $c = 13.883\text{\AA}$. There are two Mo atoms and eight Te atoms in the primitive unit-cell. All the atoms locate at the $2a$ sites of the $Pmn2_1$ space group with reduced positions of Mo: $(0.0, 0.60520, 0.50034)$, $(0.0, 0.03010, 0.01474)$, and $(0.0, 0.86257, 0.65574)$, $(0.0, 0.64045, 0.11246)$, $(0.0, 0.28997, 0.85934)$, $(0.0, 0.21601, 0.40272)$.

III. RESULTS AND DISCUSSIONS

The Td-MoTe₂ exhibits a semimetallic feature in the band structure, as shown in Figs. 2a and 2b. We refer to the lowest N -th bands (black bands) as the valence bands of a semimetal and the other higher bands (orange bands) as the conduction bands at each k -point, where N is the

number of total valence electrons. When SOC is taken into consideration, the spin degeneracy is lifted up in the band structure due to the lack of inversion symmetry. A tiny direct gap between the conduction and valence bands exist at the one fifth position of the $\Gamma - X$ line. However, near this point a pair of linearly band-crossing points exists aside from the high symmetry $\Gamma - X$ line, as shown in Fig. 2e. One point is merely 6 meV above E_F (labeled as W1) and the other is 59 meV above E_F (labeled as W2).

To validate the topology of W1 and W2 band-crossing points, we investigate the Berry curvature in the $k_z = 0$ plane calculated from the tight-binding Hamiltonian with MLWFs. The Berry curvature is integrated over all the N valence bands, by assuming a k -dependent chemical potential between the N -th and $N + 1$ -th bands at each k -point of the BZ. In Fig. 2c, one can clearly find two monopoles, W2 as a source and W1 as a sink of the Berry curvature in the positive part of BZ. It directly confirms that W1 and W2 are a pair of WPs with opposite chirality. By tracing the monopole centers of Berry curvatures, we found that the coordinates of the two WPs are W1- $(0.1024 \frac{2\pi}{a}, 0.0128 \frac{2\pi}{b}, 0)$ and W2- $(0.1001 \frac{2\pi}{a}, 0.0530 \frac{2\pi}{b}, 0)$, respectively, which is consistent with the band structure of Fig. 2e. Considering the existence of mirror symmetry in the xz (glide plane) and yz planes, four pairs of WPs

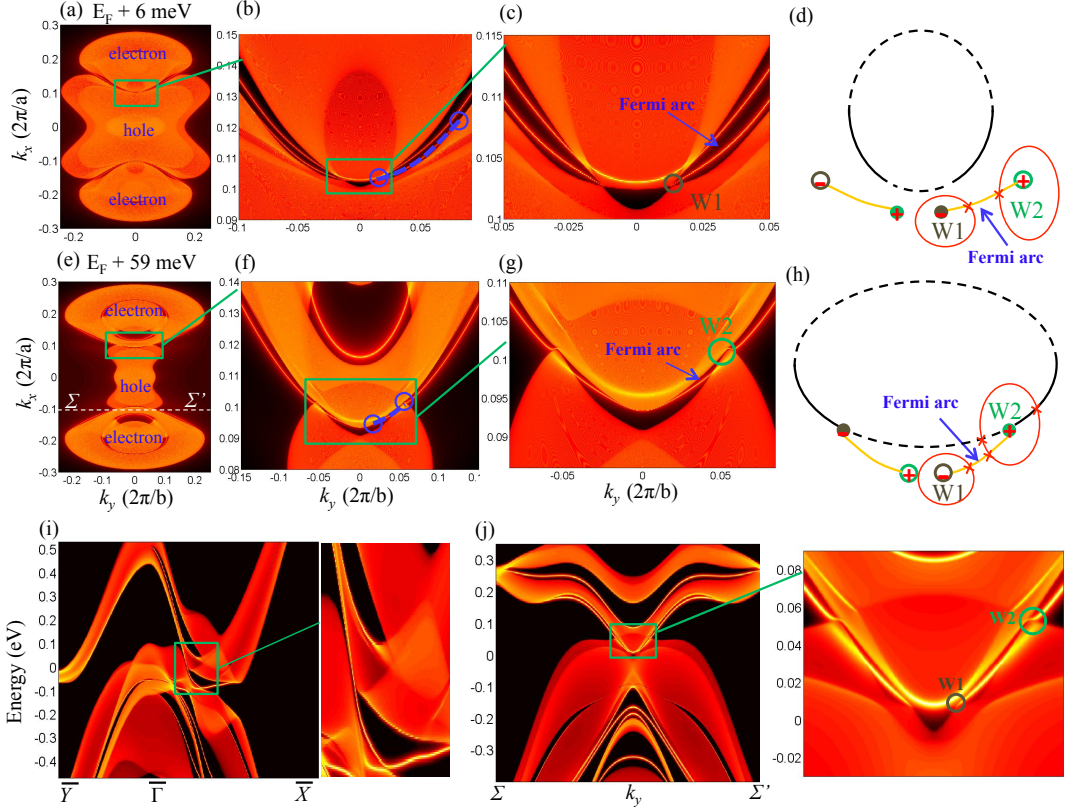


FIG. 4. Fermi surfaces and surface band structures. (a-c) Surface FS and (d) the illustration of Fermi arcs at $E_F + 6$ meV. (f-g) Surface FSs and (h) corresponding schematics at $E_F + 59$ meV. (i) Surface energy dispersion along the high symmetry lines of $\bar{Y}-\bar{\Gamma}-\bar{X}$. (j) Surface energy dispersion along the $\Sigma - \Sigma'$ crossing WPs. Brighter colors represent the higher LDOS. The exact projections of W1 and W2 are denoted as filled grey and green dots. The end points of Fermi arcs are marked as empty circles. The Fermi arcs are highlighted by dashed lines in (b) and (f).

in total can be found in the BZ (Fig. 1c).

The existence of TRS allows us to define a Z_2 topological invariant⁴⁰ on a surface with a direct energy gap. We choose a contour C that connects S , Γ and $-S$ points by crossing pairs of WPs and respects the TRS (see Fig. 1b). Since only WPs in the $k_z = 0$ plane are gapless, the C - k_z surface is gapped everywhere. Thus, we can compute the Z_2 invariant by tracing the Wannier charge centers projected to the z axis ($\langle Z \rangle$) using the non-Abelian Berry connection^{41,42}. The time-reversal partners exhibit a clear switch between the Γ and S points along the contour C during time-reversal pumping⁴³. The nontrivial Z_2 index is characterized by the odd number of times crossing of Wannier centers through the horizontal reference line in Fig. 2d. It protects the existence of helical edge states along the C projection to the surface BZ, which form part of the Fermi arcs between WPs with opposite chirality, if the k_z direction is cut to an open surface.

We note that the distance between W1 and W2 WPs is 4.2% of the reciprocal lattice, which is almost six times larger than that in WTe_2 ³¹. Therefore, the Fermi arcs

connecting W1 and W2 should be much easier to measure by ARPES in MoTe_2 than in WTe_2 . Compared to that of WTe_2 , the valence and conduction bands locate even closer to each other along the $\Gamma - X$ line, which may be attributed to the structural differences between WTe_2 and MoTe_2 . As a consequence, pairs of WPs are separated more in MoTe_2 than in WTe_2 . Given that W1 is 6 meV above E_F , only a small amount of doping is required to shift the chemical potential to the WPs.

We show the 3D energy dispersion of Weyl cones in Fig. 3. Linear dispersions exist along all momentum directions through the nodes of W1 and W2 points. Because of the weak van der Waals interactions in z direction, the Fermi velocity is much smaller in k_z direction than those in $k_x - k_y$ plane. Figures 3d-3g show the evolution of FSs in the $k_z = 0$ plane. At E_F , the electron (orange curves) and hole (blue curves) pockets are separated by a gap. On the energy increasing up, the electron and hole pockets extend and shrink, respectively. At $E_F + 6$ meV, electron and hole pockets touch each other at the W1 point, as shown in Fig. 3e. When further increasing the energy, a new gap opens at the W1 touching point

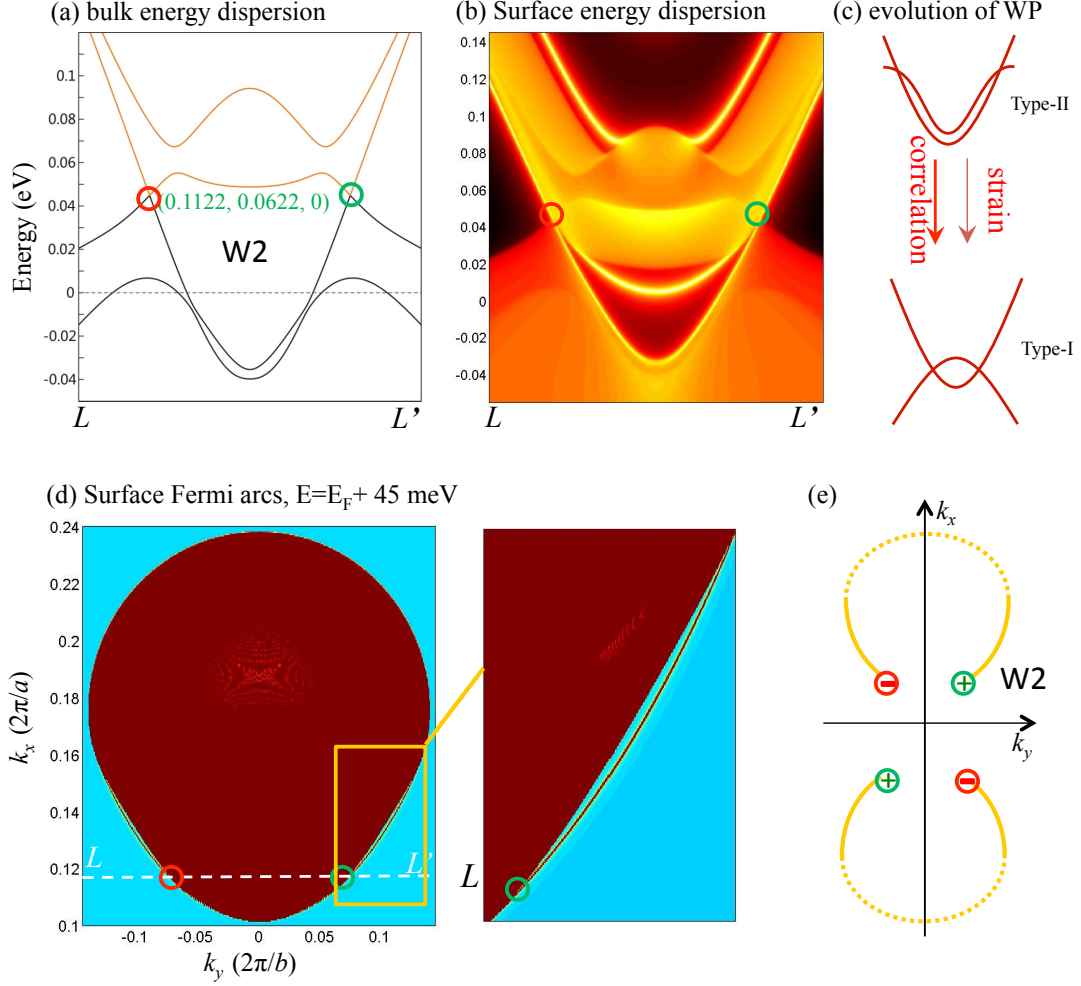


FIG. 5. Electronic structure calculated from hybrid functional. (a) Bulk band structure along two WPs in k_y directions, and (b) corresponding surface energy dispersion. (c) Schematic of WP evolution with correlation and compression strain. (d) Surface FS at the energy level of $E = E_F + 45$ meV and (e) corresponding schematics for the surface Fermi arcs. The two points of L and L' are shown in (d). The red and green circles represent WPs with opposite chirality.

until the second electron hole touching appears at the W2 point at $E_F + 59$ meV in Fig. 3f. We can clearly see that W1 and W2 WPs in MoTe_2 is formed by the touching points between electron and hole pockets in the FS, which is exactly the type-II WSM proposed in Ref. 31. Therefore, one can also expect the appearance of Fermi arcs when the E_F crosses WPs.

Next, we examine the Fermi arcs on the (001) surface. We consider a half-infinite surface using the iterative Green's function method^{44,45}. The k -dependent local density of states (LDOS) are projected from the half-infinite bulk to the outermost surface unit-cell to demonstrate the surface band structure. Except a small electron pocket near the \bar{Y} point, the FSs mainly distribute in the center region of the surface BZ. So we will focus on this region that includes all surface projections of WPs.

One can see large electron and hole pockets in the FS of Fig. 4a. The hole pockets appear near $\bar{\Gamma}$ point and the electron pockets exist in the middle of $\bar{\Gamma}$ - \bar{X} , which is consistent with the bulk band structure. As presented in Figs. 4b and 4c $E_F + 6$ meV, a Fermi arc starts from the W1 point and end at the position near the W2 point. Meanwhile a trivial FS co-exists, which is a closed circle with part merging into the bulk electron pocket. We illustrate these FSs in Fig. 4d for a simple understanding of surface states. Because the W1 and W2 WPs do not lie at the same energy, the end point of the Fermi arc cannot exactly be the surface projection of W2. As shown in Fig. 4c, the starting point is the W1 projection, while the other end point is $(0.1215\frac{2\pi}{a}, 0.0805\frac{2\pi}{b})$, relative far away from the W2 projection, just as expected. As a consequence, the length of the surface Fermi arc at $E_F + 6$ meV is much larger than the separation of

W1 and W2 points in the bulk, $\sim 7\%$ of the reciprocal lattice, which provides an advantage for the ARPES detection. When shifting E_F to the W2 position, electron pockets expands and the hole pockets shrinks, and the Fermi arcs remain in the surface BZ. At $E_F + 59$ meV, the end point of the Fermi arc becomes exactly the projection of W2 point, while the starting point shifts to $(0.0931\frac{2\pi}{a}, 0.0040\frac{2\pi}{b})$ that is close to the W1 projection. Here the Fermi arc is as long as $\sim 5\%$ of the reciprocal lattice. We note that the trivial Fermi circle now merge into the W2 point, as illustrated in Fig. 4h. But this does not change the topology of the FS.

We can understand further the Fermi arc states from the band structure with energy resolution. In Fig. 4i we can see several surface states disperse at the boundary of conduction bands and the valence bands along $\bar{\Gamma}-\bar{X}$. But their FSs are just closed circles, e.g. those in Figs. 4d and 4h. Since the line connecting W1 - W2 is almost parallel to the k_y axis, we plot the band structure along the k_y line $\Sigma - \Sigma'$ (indicated in Fig. 4e). As shown in Fig. 4j, a surface band connects to W1 and W2 in the range of ~ 5 to ~ 55 meV above Fermi level, which is consistent with the bulk band structure. This state forms the Fermi arc observed in the FS.

We should point out that the band structure of MoTe₂ is very sensitive to the structural distortion. For example, an little strain of 1% can annihilate two pairs of W1 WPs and leave only W2 WPs. Moreover, The W2 WPs turns from type-II to normal type-I as a touching point by the valence band top and the conduction band bottom, as illustrated in Fig. 5c. Considering that GGA often underestimates the correlation effect and overestimates the band inversion, we further performed band structure calculations using the hybrid-functional method (HSE06)³⁸. From the hybrid-functional calculations, we find that the original W1 WPs disappear and W2 WPs change into the type-I. New WPs lie 45 meV above Fermi level, as the band structure showing in Fig. 5a. In the surface band structures (Fig. 5b), the topological surface band connects a pair of WPs with opposite chirality, which re-

lates to the Fermi arc. As presented in Figs. 5d and 5e, at the energy $E = E_F + 45$ meV there is one Fermi curve starting from the WP in the positive zone of the 2D BZ and submerging into bulk state around the point of $(0.155\frac{2\pi}{a}, 0.125\frac{2\pi}{b})$. This Fermi curve extends out on the left side of the bulk state and finally ends at the other WP with opposite chirality. This curve is the Fermi arc that connects a pair of WPs with opposite chirality. Figure 5c illustrates the transition from type-II to type-I WSMs due to the strain or the correlation effect. Such phase transition should be considered when interpreting future experiments, due to the uncertainty of the realistic correlation effect and the lack of knowledge in the lattice contraction at low temperature.

IV. SUMMARY

In summary, we find the WSM state and reveal the topological Fermi arcs in the orthorhombic MoTe₂. By *ab initio* calculations we observe four pairs of WPs with opposite chirality lying on the $k_z = 0$ plane of the BZ. One type of WPs are just 6 meV above the E_F , and the others are at $E_F + 59$ meV, which can be accessed by slight electron doping. The spacing between WP pairs is as long as 4.2% of the reciprocal lattice, six times larger than that of WTe₂. Connecting the surface projections of WPs, topological Fermi arcs exists, which calls for the experimental verification such as by ARPES. The correlation effect or strain is expected to induce transitions from type-II to type-I WSMs in MoTe₂, which are calling for experimental verifications.

ACKNOWLEDGMENTS

We are grateful for Y. P. Qi and B. A. Bernevig for helpful discussions. This work was financially supported by the Deutsche Forschungsgemeinschaft DFG (Project No. EB 518/1-1 of DFG-SPP 1666 "Topological Insulators", and SFB 1143) and by the ERC (Advanced Grant No. 291472 "Idea Heusler").

* yan@cpfs.mpg.de

¹ GE Volovik, "Quantum Analogues: From Phase Transitions to Black Holes and Cosmology," eds. William G. Unruh and Ralf Schutzhold, Springer Lecture Notes in Physics, **718**, 31–73 (2007).

² Xian Gang Wan, Ari M Turner, Ashvin Vishwanath, and Sergey Y Savrasov, "Topological semimetal and Fermi-arc surface states in the electronic structure of pyrochlore iridates," Phys. Rev. B, **83**, 205101 (2011).

³ A A Burkov and Leon Balents, "Weyl Semimetal in a Topological Insulator Multilayer," Phys. Rev. Lett., **107**, 127205 (2011).

⁴ H B Nielsen and M Ninomiya, "Absence of neutrinos on a lattice," Nuclear Physics B, **185**, 20–40 (1981).

⁵ S L Adler, "Axial-Vector Vertex in Spinor Electrodynamics," Phys. Rev., **177**, 2426–2438 (1969).

⁶ J S Bell and R Jackiw, "A PCAC puzzle: $\pi^0 \rightarrow \gamma\gamma$ in the σ -model," Nuov Cim A, **60**, 47–61 (1969).

⁷ Reinhold A Bertlmann, *Anomalies in quantum field theory*, Vol. 91 (Oxford University Press, 2000).

⁸ H B Nielsen and Masao Ninomiya, "The Adler-Bell-Jackiw anomaly and Weyl fermions in a crystal," Phys. Lett. B, **130**, 389–396 (1983).

⁹ Gang Xu, Hongming Weng, Zhijun Wang, Xi Dai, and Zhong Fang, "Chern Semimetal and the Quantized Anomalous Hall Effect in HgCr₂Se₄," Phys. Rev. Lett., **107**, 186806 (2011).

¹⁰ Kai-Yu Yang, Yuan-Ming Lu, and Ying Ran, "Quantum Hall effects in a Weyl semimetal: Possible application in

- pyrochlore iridates,” *Phys. Rev. B*, **84**, 075129 (2011).
- 11 Adolfo G Grushin, “Consequences of a condensed matter realization of Lorentz-violating QED in Weyl semi-metals,” *Phys. Rev. D*, **86**, 045001 (2012).
 - 12 S A Parameswaran, T Grover, D A Abanin, D A Pesin, and A Vishwanath, “Probing the chiral anomaly with non-local transport in three-dimensional topological semimetals,” *Phys. Rev. X*, **4**, 031035 (2014).
 - 13 Cheng Zhang, Enze Zhang, Yanwen Liu, Zhi-gang Chen, Sihang Liang, Junzhi Cao, Xiang Yuan, Lei Tang, Qian Li, Teng Gu, Yizheng Wu, Jin Zou, and Faxian Xiu, “Detection of chiral anomaly and valley transport in Dirac semimetals,” arXiv (2015), 1504.07698.
 - 14 Su-Yang Xu, Ilya Belopolski, Nasser Alidoust, Madhab Neupane, Chenglong Zhang, Raman Sankar, Shin-Ming Huang, Chi-Cheng Lee, Guoqing Chang, BaoKai Wang, Guang Bian, Hao Zheng, Daniel S Sancez, Arun Bansil, Fangcheng Chou, Hsin Lin, Shuang Jia, and M Zahid Hasan, “Experimental realization of a Weyl semimetal phase with Fermi arc surface states in TaAs,” arXiv (2015), 1502.03807.
 - 15 B Q Lv, H M Weng, B B Fu, X P Wang, H Miao, J Ma, P Richard, X C Huang, L X Zhao, G F Chen, Z. Fang, X. Dai, T Qian, and H Ding, “Discovery of Weyl semimetal TaAs,” arXiv (2015), 1502.04684.
 - 16 L X Yang, Z K Liu, Y Sun, H Peng, H F Yang, T Zhang, B Zhou, Y Zhang, Y F Guo, M Rahn, P Dharmalingam, Z Hussain, S K Mo, C Felser, B Yan, and Y L Chen, “Weyl Semimetal Phase in non-Centrosymmetric Compound TaAs,” *Nature Physics*, in press (2015).
 - 17 B Q Lv, N Xu, H M Weng, J Z Ma, P Richard, X C Huang, L X Zhao, G F Chen, C Matt, F Bisti, V Strokov, J Mesot, Z. Fang, X. Dai, T Qian, M Shi, and H Ding, “Observation of Weyl nodes in TaAs,” arXiv (2015), 1503.09188.
 - 18 Z K Liu, L X Yang, Y Sun, T Zhang, H Peng, H F Yang, C Chen, Y Zhang, Y F Guo, P Dharmalingam, M Schmidt, Z Hussain, S K Mo, C Felser, B Yan, and Y L Chen, “Discovery of Weyl Semimetals NbP and TaP with Fermiology Evolution in Transition Metal Pnictide Family,” submitted (2015).
 - 19 Su-Yang Xu, Nasser Alidoust, Ilya Belopolski, Chenglong Zhang, Guang Bian, Tay-Rong Chang, Hao Zheng, Vladimir Strokov, Daniel S Sanchez, Guoqing Chang, Zhujun Yuan, Daixiang Mou, Yun Wu, Lunan Huang, Chi-Cheng Lee, Shin-Ming Huang, BaoKai Wang, Arun Bansil, Horng-Tay Jeng, Titus Neupert, Adam Kaminski, Hsin Lin, Shuang Jia, and M Zahid Hasan, “Discovery of Weyl semimetal NbAs,” arXiv (2015), 1504.01350.
 - 20 N Xu, H M Weng, B Q Lv, C Matt, J Park, F Bisti, V N Strokov, D gawryluk, E Pomjakushina, K Conder, N. C. Plumb, M. Radovic, G Autès, O V Yazyev, Z. Fang, X. Dai, G Aeppli, T Qian, J Mesot, H Ding, and M Shi, “Observation of Weyl nodes and Fermi arcs in TaP,” arXiv:1507.03983 (2015).
 - 21 Hongming Weng, Chen Fang, Zhong Fang, B. Andrei Bernevig, and Xi Dai, “Weyl Semimetal Phase in Noncentrosymmetric Transition-Metal Monophosphides,” *Phys. Rev. X*, **5**, 011029 (2015).
 - 22 Shin-Ming Huang, Su-Yang Xu, Ilya Belopolski, Chi-Cheng Lee, Guoqing Chang, BaoKai Wang, Nasser Alidoust, Guang Bian, Madhab Neupane, Chenglong Zhang, Shuang Jia, Arun Bansil, Hsin Lin, and M Zahid Hasan, “A Weyl Fermion semimetal with surface Fermi arcs in the transition metal monophosphide TaAs class,” *Nat. Comms.*, **6**, 7373 (2015).
 - 23 Chandra Shekhar, Ajaya K Nayak, Yan Sun, Marcus Schmidt, Michael Nicklas, Inge Leermakers, Uli Zeitler, Walter Schnelle, Juri Grin, Claudia Felser, and Binghai Yan, “Extremely large magnetoresistance and ultrahigh mobility in the topological Weyl semimetal NbP,” *Nature Phys.* (2015), doi:10.1038/nphys3372.
 - 24 Chandra Shekhar, Frank Arnold, Shu-Chun Wu, Yan Sun, Marcus Schmidt, Nitesh Kumar, Adolfo G Grushin, Jens H. Bardarson, Ricardo Donizeth dos Reis, Marcel Naumann, Michael Baenitz, Horst Borrmann, Michael Nicklas, Elena Hassinger, Claudia Felser, and Binghai Yan, “Large and unsaturated negative magnetoresistance induced by the chiral anomaly in the Weyl semimetal TaP,” arXiv:1506.06577 (2015).
 - 25 Xiaochun Huang, Lingxiao Zhao, Yujia Long, Peipei Wang, Dong Chen, Zhanhai Yang, Hui Liang, Mianqi Xue, Hongming Weng, Zhong Fang, Xi Dai, and Genfu Chen, “Observation of the chiral anomaly induced negative magnetoresistance in 3D Weyl semi-metal TaAs,” arXiv (2015), 1503.01304.
 - 26 Chenglong Zhang, Su-Yang Xu, Ilya Belopolski, Zhujun Yuan, Ziquan Lin, Bingbing Tong, Nasser Alidoust, Chi-Cheng Lee, Shin-Ming Huang, Hsin Lin, Madhab Neupane, Daniel S Sanchez, Hao Zheng, Guang Bian, Junfeng Wang, Chi Zhang, Titus Neupert, M Zahid Hasan, and Shuang Jia, “Observation of the Adler-Bell-Jackiw chiral anomaly in a Weyl semimetal,” arXiv (2015), 1503.02630.
 - 27 Zhen Wang, Yi Zheng, Zhixuan Shen, Yi Zhou, Xiaojun Yang, Yupeng Li, Chunmu Feng, and Zhu-An Xu, “Helicity protected ultrahigh mobility Weyl fermions in NbP,” arXiv (2015), 1506.00924.
 - 28 Xiaojun Yang, Yupeng Liu, Zhen Wang, Yi Zheng, and Zhu-An Xu, “Chiral anomaly induced negative magnetoresistance in topological Weyl semimetal NbAs,” arXiv (2015), 1506.03190.
 - 29 Jianhua Du, Hangdong Wang, Qianhui Mao, Rajwali Khan, Binjie Xu, Yuxing Zhou, Yannan Zhang, Jinhu Yang, Bin Chen, Chunmu Feng, and Minghu Fang, “Unsaturated both large positive and negative magnetoresistance in Weyl Semimetal TaP,” arXiv (2015), 1507.05246v1.
 - 30 Mazhar N Ali, Jun Xiong, Steven Flynn, Jing Tao, Quinn D Gibson, Leslie M. Schoop, Tian Liang, Neel Haldolaarachchige, Max Hirschberger, N. P. Ong, and R J Cava, “Large, non-saturating magnetoresistance in WTe₂,” *Nature*, **514**, 205–208 (2014).
 - 31 Alexey A Soluyanov, Dominik Gresch, Zhijun Wang, Quansheng Wu, Matthias Troyer, Xi Dai, and B. Andrei Bernevig, “A New Type of Weyl Semimetals,” arXiv (2015), 1507.01603v1.
 - 32 Yanpeng Qi, Pavel G Naumov, Mazhar N Ali, Catherine R Rajamathi, Yan Sun, Chandra Shekhar, Shu-Chun Wu, Vicky Suß, Marcus Schmidt, Eckhard Pippel, Peter Werner, Reinald Hillebrand, Tobias Forster, Erik Kampert, Walter Schnelle, Stuart Parkin, R J Cava, Claudia Felser, Binghai Yan, and Sergiy A Medvedev, “Superconductivity in the Weyl Semimetal Candidate MoTe₂,” arXiv:1508.03502 (2015).
 - 33 BRUCE E Brown, “The crystal structures of wte2 and high-temperature mote2,” *Acta Crystallographica*, **20**, 268–274 (1966).
 - 34 HP Hughes and RH Friend, “Electrical resistivity anomaly in β -mote2 (metallic behaviour),” *Journal of Physics C:*

- Solid State Physics, **11**, L103 (1978).
- ³⁵ Thorsten Zandt, Helmut Dwell, Christoph Janowitz, and Ricardo Manzke, “Quadratic temperature dependence up to 50 K of the resistivity of metallic MoTe_2 ,” *Journal of alloys and compounds*, **442**, 216–218 (2007).
- ³⁶ Georg Kresse and Jürgen Furthmüller, “Efficient iterative schemes for ab initio total-energy calculations using a plane-wave basis set,” *Phys. Rev. B*, **54**, 11169 (1996).
- ³⁷ John P. Perdew, Kieron Burke, and Matthias Ernzerhof, “Generalized gradient approximation made simple,” *Phys. Rev. Lett.*, **77**, 3865 (1996).
- ³⁸ Jochen Heyd, Gustavo E. Scuseria, and Matthias Ernzerhof, “Hybrid functionals based on a screened Coulomb potential,” *J. Chem. Phys.*, **118** (2003).
- ³⁹ Arash A Mostofi, Jonathan R Yates, Young-Su Lee, Ivo Souza, David Vanderbilt, and Nicola Marzari, “wannier90: A tool for obtaining maximally-localised Wannier functions,” *Compu. Phys. Commun.*, **178**, 685–699 (2008).
- ⁴⁰ C. L. Kane and E. J. Mele, “ \mathbb{Z}_2 topological order and the quantum spin hall effect,” *Physical Review Letters*, **95** (2005).
- ⁴¹ Alexey A. Soluyanov and David Vanderbilt, “Computing topological invariants without inversion symmetry,” *Physical Review B*, **83** (2011).
- ⁴² Rui Yu, Xiao Liang Qi, Andrei Bernevig, Zhong Fang, and Xi Dai, “Equivalent expression of \mathbb{Z}_2 topological invariant for band insulators using the non-abelian berry connection,” *Physical Review B*, **84** (2011).
- ⁴³ Liang Fu and C. L. Kane, “Time reversal polarization and a \mathbb{Z}_2 adiabatic spin pump,” *Physical Review B*, **74** (2006).
- ⁴⁴ M P Lopez Sancho, J M Lopez Sancho, and J Rubio, “Quick iterative scheme for the calculation of transfer matrices: application to $\text{Mo}(100)$,” *Phys. F: Met. Phys.*, **14** (1984).
- ⁴⁵ M P Lopez Sancho, J M Lopez Sancho, and J Rubio, “Highly convergent schemes for the calculation of bulk and surface green functions,” *Phys. F: Met. Phys.*, **15** (1985).